Reversibly Switchable Polymer Brushes with Hydrophobic/Hydrophilic Behavior: A Langevin Dynamics Study

ARTICLE *in* MACROMOLECULES · DECEMBER 2008

Impact Factor: 5.8 · DOI: 10.1021/ma8019877

4 AUTHORS, INCLUDING:

Jens-Uwe Sommer
Leibniz Institute of Polymer Research Dres…

196 PUBLICATIONS **3,119** CITATIONS

SEE PROFILE

Reversibly Switchable Polymer Brushes with Hydrophobic/Hydrophilic Behavior: A Langevin Dynamics Study

Holger Merlitz,*,†,‡ Gui-Li He,† Jens-Uwe Sommer,‡ and Chen-Xu Wu†

Department of Physics and ITPA, Xiamen University, Xiamen 361005, P. R. China, and Leibniz-Institut für Polymerforschung Dresden, 01069 Dresden, Germany

Received September 1, 2008; Revised Manuscript Received November 13, 2008

ABSTRACT: Binary polymer brushes with hydrophobic/hydrophilic behavior are forming a two-layer system with a collapsed hydrophobic and a swollen hydrophilic phase. The process of switching upon sudden change of the solvent quality is analyzed in detail for various solvent selectivities, chain lengths, and grafting densities. This process is highly reversible since after a microphase separation the chains are moving collectively inside their phase domains so that the interactions between chains of different species are diminished. The thickness of the collapsed layer does not scale linearly with the chain length N, an unexpected result which is discussed in the paper. The switching relaxation times display a scaling of N^2 like Rouse relaxation and not of N^3 like vertical relaxation times in equilibrium.

1. Introduction

The creation of functional materials with extreme properties has become a key issue of modern nanotechnology. Countless potential fields of application have been spotted, including adhesives which stick on any surface,[1] superhydrophobic coatings,[2] or antifriction coatings,[3] to cite just a few of them. Functional surfaces that are able to adopt their properties to their environment are moving another step further: A textile with superhydrophobic properties may be useful in rainy weather but also difficult to dye or to wash. Coatings that can be switched reversibly from hydrophobic to hydrophilic behavior would therefore offer a diverse range of applications. One promising approach to achieve this goal is the employment of a binary polymer brush, of which one component is made of hydrophilic and the second of hydrophobic polymers. The investigation of characteristic properties and the switching dynamics of such a binary brush is the goal of the present paper.

Mixed polymer brushes have been approached theoretically by Marko and Witten, who analyzed the phase diagrams of these systems using self-consistent-field theory (SCF) in the strong stretching limit.[4,5] Their approach was later generalized to brushes of arbitrary grafting density by Müller, who has observed various forms of microphase separation of different morphologies.[6] His findings were verified experimentally by Minko et al. using atomic force and X-ray photoemission microscopy.[7] The reversible switching of a mixed polymer brush was first observed in experiment by Sidorenko[8] and analyzed in detail by Minko[9] and Lemieux.[10] Motornov et al. have recently applied this technology to modify the surface of colloids in order to create stimuli-responsive ("smart") nanoparticles,[11] and Chervanyov et al. have studied polymer adsorption onto selective mixed brushes using SCF techniques.[12]

The SCF approach does predict highly regular patterns for the microphase separation of mixed brushes due to the neglect of thermal fluctuations. Those are taken into account by computer simulations, and Soga et al. were among the first to simulate the microphase separation of binary brushes at various solvent qualities.[13] Later, Wenning et al. have carried out Monte Carlo simulations to investigate the structure of mixed brushes as a function of the grafting pattern,[14] and Santer et al. have recently simulated the influence of the particular grafting morphology on the microphase domain structure at different solvent properties.[15]

The primary scope of the present work is not to study the lateral patterns of microphase domains but rather the vertical separation of the two phases, which emerge whenever the solvent is sufficiently selective, and their mechanism and dynamics of switching. In recent works, Yin et al. have studied the vertical phase separation of triblock copolymers using simulated annealing on a lattice,[16] and Mao et al. have created a reversibly switching DNA layer with hydrophilic/hydrophobic behavior in the laboratory.[17] Our present work is using Langevin dynamics, being able to deliver physical time scales for off-lattice systems with implicit solvent at finite temperature, thereby covering both dissipation and thermal fluctuations. In section 2 the polymer model parameters are explained, and in section 3.1 we present the simulation procedures. Section 3.2 discusses the structural properties of the system under various conditions, and in section 4 the dynamics of switching is analyzed. A summary of our findings is presented and discussed in section 5.

2. Brush Model and Simulation Tool

The polymers were created as a coarse-grained bead−spring model without explicit twist or bending potential; i.e., the bonds were freely rotating and freely jointed within the limits as set by excluded volume interactions with nearby monomers. The "spring" was a finite extensible nonlinear elastic (FENE) potential.[18] The beads represent spherical Kuhn monomers which interact via a shifted Lennard-Jones (LJ) potential

$$U_{\mathrm{LJ}}(r) = 4\epsilon\left[\left(\frac{d}{r}\right)^{12} - \left(\frac{d}{r}\right)^{6} - \left(\frac{d}{r_{\mathrm{c}}}\right)^{12} + \left(\frac{d}{r_{\mathrm{c}}}\right)^{6}\right] \qquad (1)$$

where d stands for the bead diameter and ϵ defines the strength of the interaction. The parameter r_{c} is the cutoff distance and of particular relevance for this work. It is easily verified that without any cutoff ($r_{\mathrm{c}} \rightarrow \infty$) this potential has got a minimum at $r_{\mathrm{min}} = 2^{1/6}d$ with the depth $U_{\mathrm{LJ}}(r_{\mathrm{min}}) = -\epsilon$. In turn, once a cutoff $r_{\mathrm{c}} = 2^{1/6}d$ is implemented, the attractive contribution to this potential is eliminated, and in this way monomers inside an athermal solvent are simulated. On the other hand, a far cutoff retains the attractive part of the potential and allows to simulate various solvent qualities, depending on both ϵ and the temperature of the system. In this way, ϵ takes over the part of the

* To whom correspondence should be addressed.
† Xiamen University.
‡ Leibniz-Institut für Polymerforschung Dresden.

10.1021/ma8019877 CCC: $40.75
Published on Web 12/10/2008

solvent selectivity within this implicit solvent model. Unless athermal solvent has to be simulated, it is common practice to select $r_c = 2.5d$ in order to keep the number of pair interactions on a tolerable level.

In order to create a binary brush, two homopolymer species were end-grafted onto a planar surface which defined the $x-y$ plane at $z = 0$. Here, a 9−3 type LJ wall potential was implemented

$$U_{\text{wall}} = \epsilon\left[\frac{2}{15}\left(\frac{d}{r}\right)^9 - \left(\frac{d}{r}\right)^3\right] \tag{2}$$

including a cutoff at the minimum (and being subsequently shifted up to eliminate any negative contribution to the total potential) which prevented the polymers from passing through the substrate. The two polymer species consisted of monomers which henceforth shall be denoted as **A** type and **B** type, respectively, which were grafted onto the substrate in a Cartesian pattern. The **A** species was exposed to a poor solvent (simulated with a long cutoff distance for the **A**−**A** interaction potential), and the **B** species was in athermal solvent, or vice versa. Throughout the paper, the species were incompatible; i.e., the **A**−**B** interaction did not contain any attractive contribution. The wall potential did not distinguish between both species, with the exception of a single simulation with full wetting substrate, and boundary conditions were periodic in both x and y directions.

The simulations were carried out using the open source LAMMPS molecular dynamics package.[19] In this paper, the LJ system of units is used. It is defined using a model polymer with a LJ pair potential, featuring a bead size $d = 1$ (one length unit), a potential depth $\epsilon = 1$ (one energy unit), and a mass $m = 1$ (one mass unit). The temperature is then normalized to that energy unit (using a Boltzmann constant $k_B = 1$), and the time unit is $\tau_{LJ} = d(m/\epsilon)^{1/2}$, which is the oscillation time of a monomer inside the LJ potential, at small amplitudes so that the harmonic approximation is valid. Note that, throughout this paper, all units are LJ units which are normalized to this model polymer, even when the potential depth ϵ is varied to deviate from unity. The grafting density σ of the polymer brush is defined as the (average) number of grafted monomers per unit area. Since in our case the bead size was fixed to $d = 1$, a grafting density of $\sigma = 1$ implies a closely packed system which would form a crystal.[20] The choice of the bond force parameters led to an average bond length of $0.97d$.

The equation of motion of any nongrafted monomer in the implicit solvent (neglecting any hydrodynamic interaction) is given by the Langevin equation:

$$m\frac{\mathrm{d}^2\mathbf{r}_i}{\mathrm{d}t^2} + \zeta\frac{\mathrm{d}\mathbf{r}_i}{\mathrm{d}t} = -\frac{\partial U}{\partial \mathbf{r}_i} + \mathbf{F}_i \tag{3}$$

where $m = 1$ is the monomer mass, $\mathbf{r}_i$ the position of the ith monomer, U is the total conservative potential, and $\mathbf{F}_i$ is a random external force without drift and a second moment proportional to the temperature and the friction constant ζ. In our simulations, the temperature $T = 1$, a time step $\Delta t = 0.003\,\tau_{LJ}$, and the friction coefficient $\zeta = \tau_{LJ}^{-1}$ were implemented. The applied friction leads to an overdamped motion on the length scale of the bead size, so that the dynamics of monomers is diffusive as it should be with a polymeric system inside a solvent.

3. Results

3.1. Simulation Procedure. The brushes were created as 24 × 24 arrays of alternating **A** and **B** type polymers with periodic boundaries in both horizontal directions and a grafting density of $\sigma = 0.116$. (Throughout the paper, grafting densities refer to densities of both polymer types without distinction of species.) Simulations were carried out for three different degrees of polymerization ($N \in \{32, 64, 128\}$) and three different solvent selectivities, represented by the potential depth of the LJ pair potential eq 1, using $\epsilon \in \{0.25, 0.5, 1\}$. Additionally, for $\epsilon = 0.5$ and $N = 64$, a series of different grafting densities $\sigma \in \{0.082, 0.116, 0.16, 0.25, 0.34\}$ were simulated. In each simulation, the brush was first fully relaxed such that both species were separated into two vertical layers, as shown in Figure 1 (left). Then, both species were swapped; i.e., the **B** polymers were facing a good solvent instead of a poor solvent, and vice versa for species **A**. This was causing a switch of both layers. After another relaxation period, the species were swapped again and subsequently relaxed once more, in order to verify that the entire process was fully reversible. Hence, each simulation run delivered three values for the brush heights for each of the layers, which were averaged, and the variations were used to estimate the errors. Furthermore, each simulation delivered two switching times for both the up−down and the down−up switch, which again were averaged separately, and the respective variations were used to estimate their errors.

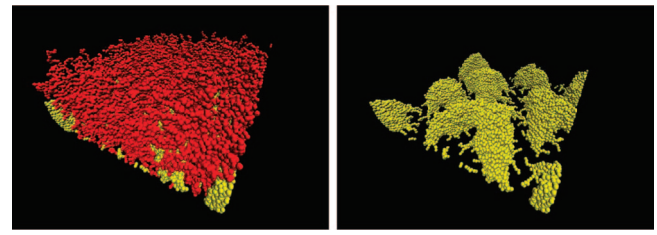

Figure 1. Binary brush after complete relaxation. The hydrophilic species (red) is exposed to the solvent and forming a homogeneous upper brush layer (left). The hydrophobic layer (yellow) is creating an inhomogeneous layer with a droplike clusters (right). Here, the polymer length $N = 64$, the selectivity $\epsilon = 1$, and the grafting density $\sigma = 0.116$.

3.2. Structural Properties of the Brush. There exist several approaches to define the height of a brush layer. As long as the brush is placed inside a good solvent and the chains are, in average, well stretched, the vertical coordinate of the end-monomer may be used as a measure for the layer thickness. This strategy fails once the brush is in poor solvent and forms a collapsed high-density layer, in which the end-monomer of each chain has got a random position. If the brush is large enough to allow for the definition of vertical density profiles for a single conformation, then the brush height may be defined using the drop of this profile near the surface. This method, however, is not very accurate and prone to significant statistical fluctuations. It is therefore more reliable to use the center of mass of the brush layer as an indicator for its thickness, and being an integrated quantity, its statistical fluctuations are small. Here, one just has to keep in mind that the true layer thickness would roughly be twice as large as its vertical center of mass position. As an alternative, one may consider the vertical component of the radius of gyration, averaged over all chains, which corresponds to the fluctuation of the chains about their center of mass. However, in contrast to the free chain case, as a result of the half-plane restriction of the substrate, these fluctuations are not symmetric, and being a second moment quantity, they emphasize the extreme deviations such that the statistical error is larger than that of the center of mass. For our investigation we will therefore use the vertical center of mass coordinate to define the layer thickness, which is denoted as H throughout the paper.

Scaling theory would predict a brush thickness proportional to the degree of polymerization N, regardless of the solvent

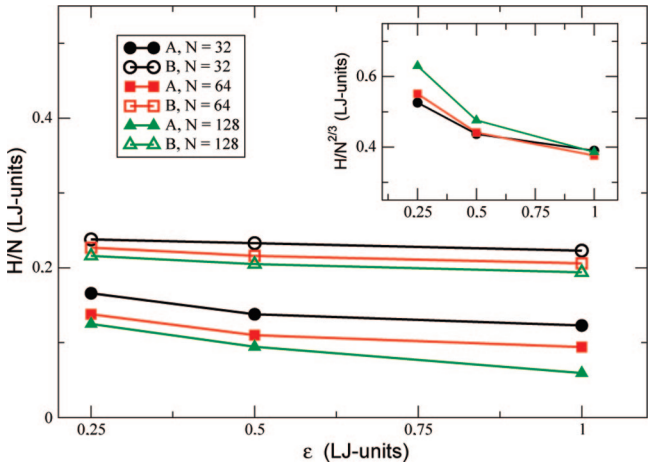

Figure 2. Thickness of both polymer layers as a function of the solvent selectivity ϵ, scaled with the chain length N. **B** stands for the athermal solvent species, and **A** is the lower, poor solvent layer. Inset: the poor solvent layer displays an (empirically fitted) $\sim N^{2/3}$ scaling at high solvent incompatibility due to finite size effects.

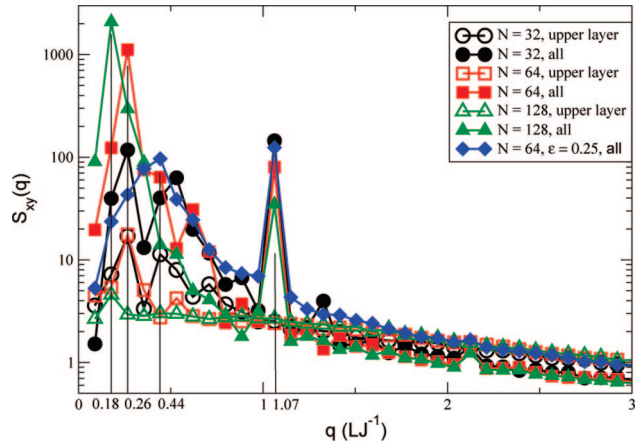

Figure 3. Structure factor for binary brushes at selectivity $\epsilon = 1$. Solid symbols are covering the entire brush and blank symbols only the upper half of the brush which contains the good solvent component. For comparison, the diamonds show the result of the $\epsilon = 0.25$ simulation where the drop structure had almost disappeared. The upper layers display a negligible signal.

quality.[21] Once the measured heights of brushes of various polymer lengths are rescaled with N, the results should therefore fall on top of each other. Figure 2 demonstrates that this condition is approximately satisfied by the upper, good solvent layer (blank symbols). Additionally, for this layer, hardly any dependence upon the solvent selectivity ϵ is visible, a natural consequence of the athermal solvent model applied to that polymer species.

The poor solvent layer (solid symbols), however, behaves differently: First, a significant dependence of its thickness on the solvent selectivity is visible. At this point it is essential to mention that the term *poor solvent* is actually misleading for the case $\epsilon = 0.25$. We have carried out simulations on free chains at different temperatures to verify that the theta temperature for this species would be

$$\Theta(\epsilon = 0.25) = 0.75 \pm 0.1 \tag{4}$$

Our simulations were done at $T = 1 > \Theta(\epsilon = 0.25)$, which is already above that theta temperature. In the case of the binary polymer system, however, one has to be aware that the presence of the second species does not leave the theta point unaffected, so that the above-defined theta temperature may serve only as a rough estimate for the status of the (lower) poor solvent layer inside the brush. Moreover, entropic restrictions due to grafting do also change the effective theta point.[22] Since the theta temperature increases about linearly with ϵ, only the simulations at $\epsilon = 1$ were definitely well below the theta point ($\Theta(\epsilon = 1) \approx 3$) and featuring true poor solvent layers. We shall therefore conclude that the modification of solvent quality while moving through the theta point was responsible for the variation of the lower layer thickness in Figure 2.

Another important observation is that the H/N scaling is not satisfied for the poor solvent layer. Instead, at high solvent selectivity, an apparent scaling of $\sim N^{2/3}$ can be determined empirically (inset of Figure 2), which is only gradually turning into the linear scaling regime with diminishing ϵ. This scaling is not related to any scaling theory and might be attributed to finite chain length and variations of scaling variables as will be discussed below.

Figure 1 (right) displays the brush ($N = 64$, $\epsilon = 1$) after removal of the upper layer so that the poor solvent layer becomes visible. It is obvious that this layer did not create a flat and homogeneous film on top of the substrate, but instead formed droplike clusters. On the first sight, one might be tempted to address this phenomenon to the monomer−substrate interaction because the wall potential did not include any attractive component. However, it was easily verified that after the introduction of such a short-range attraction (by increasing the cutoff used in eq 2 to 2 LJ units and using the same interaction parameter $\epsilon = 1$) the observed clusters did not disappear; i.e., a complete wetting of the substrate could not be achieved. This indicates that the incompatibility between both polymer species was still dominant under these conditions, and it would require a strong polymer−substrate attraction to break up the clusters. Recent studies using simulated annealing have obtained a plethora of different morphologies which have been classified in terms of a phase diagram.[16]

It should be noted that the size distribution of these droplets is a function of the degree of polymerization. In order to quantify this claim, we compute the lateral structure factors for the brushes at $\epsilon = 1$ and for different N. For a given scattering vector $\mathbf{q}$, the structure factor $S(\mathbf{q})$ is defined as

$$S(\mathbf{q}) = \frac{1}{N_m}\left\langle \sum_{j,k=1}^{N_m} \sigma_j \sigma_k \exp[i\mathbf{q}(\mathbf{r}_j - \mathbf{r}_k)] \right\rangle \tag{5}$$

Here the sum runs over all N_m monomers with coordinates $\mathbf{r}_j$ inside the particular probe to be investigated. The quantities σ_i are taking the values ± 1, depending on the monomer species, and generate the contrast between both chain species. The periodic boundary condition of the simulation box in both lateral directions is limiting the choices for the scattering vector[23] to

$$\mathbf{q}_{xy} = \frac{2\pi}{L}(n_x, n_y), \quad 0 \le n_i \le L \tag{6}$$

with L being the box size. For simplicity, we have analyzed the set of scattering vectors q_x and q_y separately and then averaged the resulting scattering functions. Vertical directions were excluded from the analysis, thereby restricting S_{xy} to cover only the dimensions of structures in the x and y directions. The analysis was done for both the entire brush and, as a comparison, for the upper layer of the brush which exclusively contained the good solvent species. In either case, several hundreds of conformations were analyzed, and the results were averaged.

The results are presented in Figure 3. Generally, the upper layer (blank symbols) did not display any significant structure, indicating that the polymers inside this region of the brush did occupy the brush volume almost homogeneously. Once the

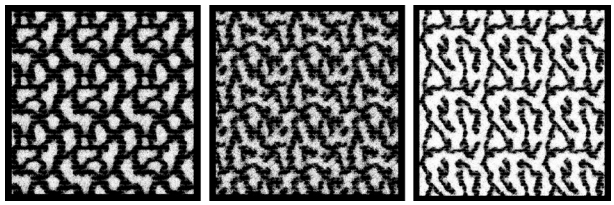

Figure 4. Domain structures created by the poor solvent component of the $N = 64$ brushes (view from top onto the $x-y$ plane; the poor solvent species is white, and the second species is omitted). At low grafting density ($\sigma = 0.116$) and high selectivity ($\epsilon = 1$), the chains are creating isolated drops (left). When reducing the selectivity to $\epsilon = 0.5$, the drops begin to connect to form stripelike domains (center). An increase of the grafting density to $\sigma = 0.25$ creates similar domains even at high selectivity $\epsilon = 1$ (right). In order to enhance the visibility of the patterns, periodic images of the brushes have been added.

lower regions of the brush are included into the analysis (solid symbols), the situation is changing. First, there is a well pronounced peak at $q = 1.07$. The corresponding spacial distance is $2\pi/q = 5.88$, which is the distance at which monomers of same type are grafted onto the substrate. Apart from this trivial signal, the positions of the main peaks display a variation with the polymer size: For $N = 128$ the maximum is near $q = 0.18$, for $N = 64$ at 0.26, and the system $N = 32$ has got a much weaker signal with maxima near 0.26 and 0.54. These peaks correspond to spacial extensions of the domains between roughly 35 LJ units ($N = 128$), 24 LJ units ($N = 64$ and first peak at $N = 32$), and 12 LJ units (second peak at $N = 32$), well in between the dimension of the grafting distance (5.88 LJ units) and the box size (71 LJ units).

It is interesting to note that the scattering intensity of the $N = 64$ chains at low solvent selectivity ($\epsilon = 0.25$, diamonds) is 1 order of magnitude lower when compared with the same system at high solvent selectivity (squares). Its rather broad peak has got a maximum near $q = 0.44$, which corresponds to spacial domain sizes around 14 LJ units. Here, being near the theta point of poor solvent species, both species have already partially intermixed so that the lateral domain structures have become diffuse.

With these results it is possible to qualitatively explain the breakdown of linear scaling as observed in Figure 2 for the poor solvent layer: Here, the polymers do not form a flat, homogeneous film on top of the substrate, but clusters with size distributions which themselves are functions of the chain length, hence causing corrections to the asymptotic scaling behavior which should be linear in N for very long chains. Additional corrections arise due to changes of scaling variables, namely chain overlap and average interaction per chain. The latter effects could, in principle, be eliminated by keeping the product of grafting density and mean-square chain extension as well as the interactions per chain fixed, while the chain length is increased. This approach would be difficult to realize in experiment, however, and shall not be followed up in the current work.

In order to discuss the lateral pattern of the poor solvent layer, Figure 4 is displaying three typical examples. The left panel shows the same pattern as Figure 1 (right), but seen from above and with some periodic images added so that the structure becomes more obvious. The clusters of polymers at $\sigma = 0.116$ and $\epsilon = 1$ are clearly distinguishable and form droplike structures. Once the solvent selectivity is reduced to $\epsilon = 0.5$, then these clusters begin to grow together to create a stripelike pattern. A further decrease of ϵ (which would imply a reduction of the incompatibility of the lower phase both with the solvent and with the second species) would shift the polymers from the poor solvent domain to the good solvent domain where the pattern does gradually disappear. On the other hand, an increase

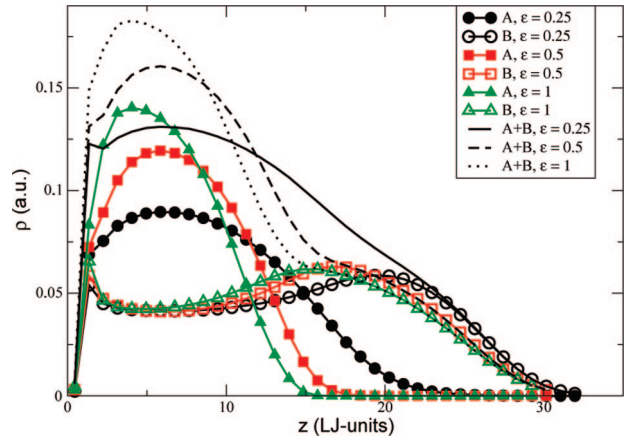

Figure 5. Vertical densities (arbitrary units) of the brushes of $N = 64$ at different solvent selectivities. Here, the **A** species (solid symbols) forms the poor solvent layers, whereas the **B** species (blank symbols) creates the upper, good solvent layer. The lines represent the total densities.

of the grafting density to $\sigma = 0.25$ does again create stripelike patterns even at high solvent selectivity $\epsilon = 1$ (right panel). For this simulation, we have increased the number of grafted polymers to 36×36 in order to leave the box size invariant and avoid any finite size effects which could influence the domain structure.

These results indicate that it is possible to distinguish different phases of the poor solvent layer, depending on solvent quality, grafting density, and also chain length (data not shown). It should be mentioned that earlier theoretical studies have already predicted various morphologies of similar domains in the situation of nonselective solvents,[6] which have been qualitatively verified in experiment.[7] Quite in analogy to our observations, a regular pattern of "dimples" (corresponding to the droplike clusters in our simulation) were found in the case of strong incompatibility of the two polymer species, and these transformed into regular "ripples" (corresponding to our stripelike structures) at lower incompatibility. The patterns obtained by Müller were highly regular because he had used SCF theory which neglected the thermal fluctuations.[6] In any case, the fundamental differences between both systems (i.e., selective vs nonselective solvent) permit merely a qualitative comparison of his results with our observations.

Further interesting properties of the binary brushes are the vertical density distributions of their both layers. As can be seen in Figure 5, there exists a significant variation of the poor solvent layer (solid symbols) with the solvent selectivity. At $\epsilon = 1$, this layer is quite compact and restricted to coordinates below 15 LJ units. With decreasing selectivity ϵ, this layer is beginning to swell. As was already discussed earlier in this section, at $\epsilon = 0.25$ the system temperature ($T = 1$) was actually above the theta point $\Theta(\epsilon = 0.25) \approx 0.75$ of the corresponding homogeneous system, and the **A** species layer was already partially swollen, though not as much as its athermal counterpart **B**. The lateral structure factor at $\epsilon = 0.25$ did exhibit much less pronounced peaks, indicating that the drop structure which was observed at $\epsilon = 1$ had partially diffused and the polymers were forming a somewhat collapsed but otherwise almost homogeneous layer on top of the substrate (shown as diamonds in Figure 3).

The athermal solvent layer (blank symbols in Figure 5) remained almost unaffected of the variations of the poor solvent layer, though not entirely. It is obvious that there must exist a certain coupling between both polymer layers because the excluded volume interactions between the collapsed and the swollen layer are mutually affecting the statistical properties

of both polymer species. For this reason, the scaling of the upper brush layer as shown in Figure 2, blank symbols, is not as perfectly linear in N as it would be in case of homopolymer brushes in athermal solvent.[24]

When comparing the total vertical density distributions (plotted as lines in Figure 5), a transition from a two-phase system (at high solvent selectivity) to a single-phase system (at $\epsilon = 0.25$) is observable. In the first case, the density profile displays a sharp kink at the surface of the dense layer, which disappears in the latter case where the lower layer is already swollen to form a diffuse transition layer with the athermal species.

4. Relaxation Dynamics of Switching

Another feature to be addressed is the dynamics of the brush relaxation during the switching process. The actual time scales may not be of immediate interest for technical applications because there the actual process of switching is far more complex when compared to the approximations of the current work: The brush might first be washed in order to remove one solvent type and then dipped into the second, complementary solvent. It is by no means intended to simulate these processes explicitly in the current work. Instead, it is assumed that one solvent type is instantaneously replaced with another solvent, and this is achieved by swapping the pair-interaction potentials of both monomer species. Although the resulting switching times are not likely to be realistic, the fundamental mechanism of this process and its scaling with the system parameters are assumed to exhibit universal features.

Figure 6 (upper part) displays the process of switching after the both monomer species had swapped their interaction potentials at $t_{sw} = 45\,000$ LJ times. This relaxation was fitted as a single exponential decay mode of the form

$$H(t) = \exp\left(-\frac{t - t_{sw}}{\tau_s}\right)(H_1 - H_2) + H_2 \qquad (7)$$

where τ_s defines the relaxation time of the switch, and the heights H_1 and H_2 were free fit parameters. This simple approach did reproduce the relaxation dynamics of the brushes quite accurately, particularly in the case of shorter chains, but even the $N = 128$ brushes could be fitted with reasonable accuracy. A deviation from the single-exponential decay was usually observed during the very initial phase of the up-switch. The corresponding plot (circles in Figure 6) exhibits a sudden rise of the layer thickness, indicating another, much faster relaxation mode being active here, probably related to the short-range repulsion of monomers just after their attractive interaction was eliminated. These initial data points had therefore been excluded from the process of fitting. The resulting asymptotic heights H_1 and H_2 are not suitable to fit the actual layer thickness reliably; these heights are found to much higher accuracy by direct measurements on brushes in equilibrium.

The three plots in the center part of Figure 6 display snapshots of the same brush at different stages of the switching. Shortly after the change of the solvent, the upper, initially good solvent layer (red, left image) is collapsing and breaking up. The initially poor solvent layer (yellow) is still forming clusters inside the lower layer of the brush. Gradually, the red layer is contracting to form domains which are sinking deeper into the brush, while the yellow clusters are breaking through and moving up (central image). Later on, the yellow domains are swelling into the good solvent while the red clusters have retreated back inside the brush (right image). Even later, the brush will reach a new equilibrium, and the yellow layer will be entirely swollen to form a disordered and homogeneous layer on top of the brush. The collective movement of entire domains during the switch

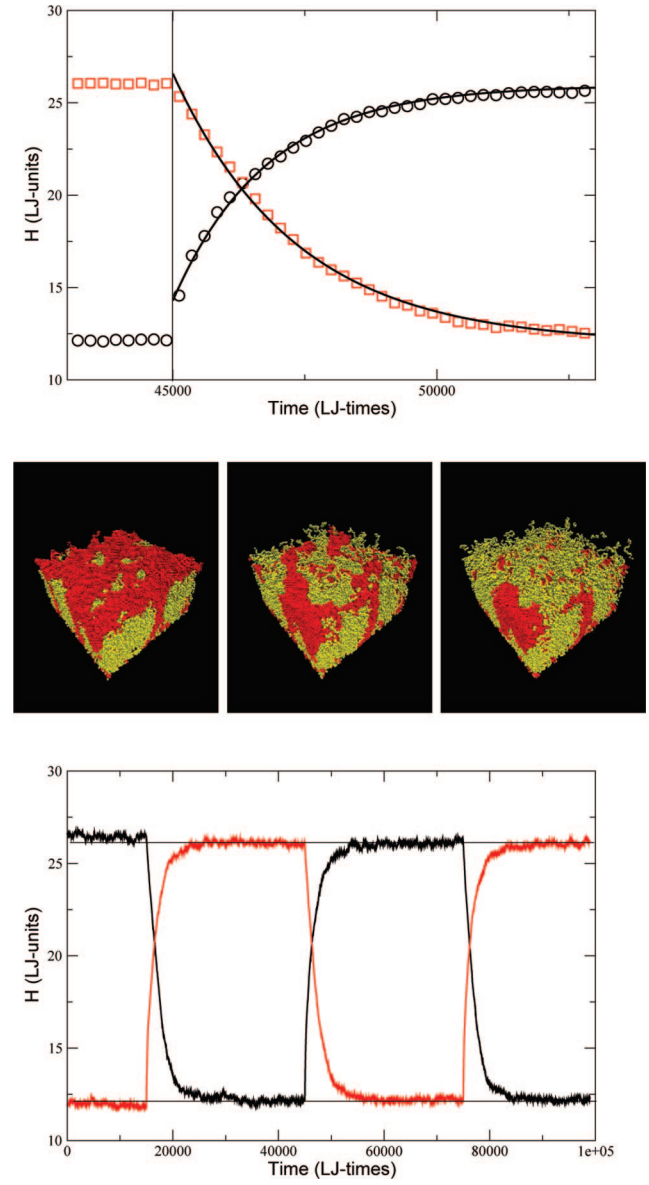

Figure 6. Upper: a switch of two polymer layers after swapping their monomer−solvent interaction at $t_{sw} = 45\,000$ (vertical line). The solid curves are single-exponential fits to determine the relaxation times. In this system, $N = 128$ and $\epsilon = 0.5$. Center: snapshots of the brush during the switch. Lower: the switching is reversible.

implies that the penetration of individual chains through the respective incompatible layer remains an exception. As a result, the switching process remains highly reversible even on the relatively short time scales investigated in our simulations.

In this context, it should be pointed out that such a switch process would always be reversible, from a thermodynamics point of view. However, chains which belong to the good solvent phase might get captured and trapped inside the poor solvent phase. If this phase is in a melt state, as is the case in our simulations, then those chains are able to escape within moderate time scales. This process might still be slow enough for the reversibility of the switch being violated on short time scales for kinetic reasons and hence affecting certain technical applications that ask for a rapidly switching surface. If the poor solvent species were going through a glass transition, then chain capture would even become permanent until the next switch, which in the worst case could affect the functionality of the brush.

In order to quantify the degree of short-term reversibility, the lower part of Figure 6displays three consecutive switches

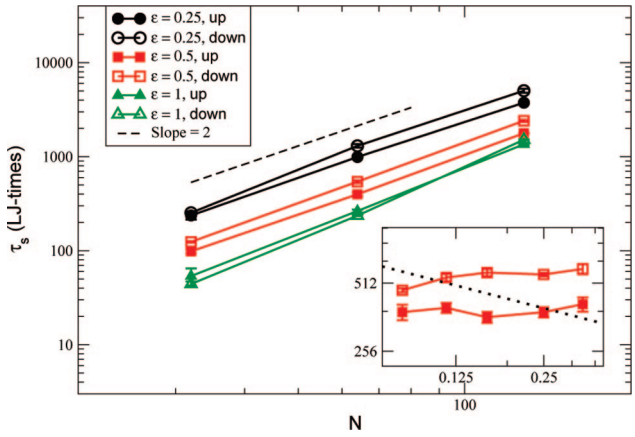

Figure 7. Brush relaxation times τ_s as obtained with the fit of eq 7. The solid symbols stand for the up-switch, i.e., the collapsed layer swelling into the good solvent, and the blank symbols stand for the down-switch, i.e., the swollen layer collapsing inside the poor solvent. The dashed line is the $\sim N^2$ Rouse scaling law. Inset: the same relaxation times for $\epsilon = 0.5$ as a function of the grafting density σ. The dotted line is the $\sim\sigma^{-1/3}$ scaling of eq 8.

of the binary brush. After the first switch, the equilibrium heights of the layers remain unaffected by further switches. Only the initial heights, measured after the brush had equilibrated and prior to the first switch, are different by a tiny margin. In this case, the history of the system, being equilibrated from the initial conformation, where the chains were linear sticks, was different. During the first switch, a small fraction of chains that belong to the upper, athermal layer, is trapped inside the poor solvent layer, so that the height difference between both layers is reduced by roughly 3%, but this value does not change any further during the following switches. In summary, we observe a certain, small fraction of chain entanglement after the initial switch, which is verified to be nonaccumulative and hence not affecting the reversibility of rapidly repeating switch events.

For a measurement of the relaxation times, two switch events were analyzed for each system, and the resulting numbers were averaged, using their standard deviation as an estimate for the statistical error. Figure 7 contains the relaxation times as a function of the chain length. In general, the times for the up-switch and down-switch did not coincide. This is not surprising, since the mechanisms involved in these two processes are fundamentally different: If a polymer moves initially inside a good solvent, i.e., in a swollen state, and suddenly the interaction is modified to simulate a poor solvent, then it is the attractive monomer−monomer pair interaction which begins to pull the polymer down. Once a polymer in poor solvent is exposed to a good solvent, however, then it is its thermal fluctuations which facilitate the swelling of the chain; i.e., here entropic forces are driving the layer rather than enthalpic forces. The simulations indicate that, as long as the solvent selectivity remains moderate, i.e., at $\epsilon = 0.25$ and $\epsilon = 0.5$, the entropy driven up-switch is somewhat faster than the enthalpy driven down-switch. At high solvent selectivity, i.e., $\epsilon = 1$, the differences for both relaxation times are diminishing. However, in a binary brush, the both brush layers are never fully decoupled from one another. Once the enthalpic interaction is modified, it affects not only the down-switch dynamics but, along with the density shift of the layer, the up-switch dynamics as well. Figure 7 might, at first sight, indicate an inversely linear relation between the relaxation time and the solvent selectivity ϵ, but a corresponding rescaling of the data would in fact deliver just a very rough alignment and deviations from this scaling law are significant.

Apart from differences between the up- and down-switching times, the plot clearly indicates a scaling of N^2 with respect to the chain length. Since the structural changes during the switch do involve length scales comparable to the molecular extension, the time scale of this process is dictated by Rouse relaxation[27] which is leading to the observed scaling. To be precise, the relaxation time does follow the Rouse time multiplied with a rather complicated scaling function, which contains the chain interaction and creates the different prefactors for both up- and down-switching times. It should be noted that this process is fundamentally different from the vertical relaxation of chains inside an equilibrated brush, whose time scales have been shown to grow $\sim N^3$ both theoretically and via computer simulation.[24,28,29] The N^2 scaling of the switching process is therefore a clear indication for a nonequilibrium process, and the characteristic time scales are in fact significantly shorter than the corresponding equilibrium relaxation times found in ref 24.

Finally, relaxation times as a function of grafting density have been analyzed. In this context, Halperin has suggested characteristic times associated with the longitudinal breathing modes of a flat homopolymer brush.[21] Following an earlier work by deGennes[25] and based on the Alexander model,[26] Halperin was balancing the elastic spring forces of the chains with the viscous friction of the solvent to obtain

$$\tau_l \sim N^2\sigma^{-1/3} \tag{8}$$

The N^2 scaling is identical to the Rouse relaxation and hence not specific enough to support the model. The scaling of τ_s with the grafting density, however, could not be verified in the simulations: The inset of Figure 7 displays the switching times of the $N = 64$ brushes at $\epsilon = 0.5$ as a function of the grafting density, and the dotted line would follow the predicted $\sim\sigma^{-1/3}$ scaling. The data indicate that the relaxation times of the brushes are essentially invariant of the grafting density or, perhaps, even slightly increasing. This failure should not be regarded as a deficiency of Halperins model, however. Instead, the application of this model to the current system appears to be inadequate. It is obvious that the breathing modes were based on approximations, only valid for small oscillation amplitudes around the equilibrium height. In contrast, the switching of a binary brush is a nonequilibrium process and involves much larger amplitudes beyond any harmonic approximation, making it unsuitable to be described as a breathing mode.

5. Conclusion

At first sight, the vertical switching of two incompatible layers of grafted polymers appears to be a delicate process: Upon changing the solvent quality, both chain layers have to move through each other in opposite directions. Such a process might be expected to create a considerable disorder of the vertical demixing, which would lead to a significant slowdown of relaxation and eventually even to a quasi-irreversible disfunction of the brush. In contrast, our simulations, carried out with different chain lengths and also covering various grafting densities, generally displayed a high degree of reversibility of the switching even on short time scales.

The reason for that is revealed in Figure 6: The two layers do not penetrate each other on the level of individual chains. Instead, the incompatible chain species are microphase separating and forming clusters, and it is these domains which are swapping their vertical positions. A friction, and hence the danger of trapping good solvent chains inside the poor solvent layer, is limited mostly to the boundaries of these clusters and leaves the reversibility of the process almost unaffected.

At high solvent selectivity, both vertical layers behave like two different phases, and the vertical density distributions in Figure 5 display a kink at the phase boundary. In lateral directions, the poor solvent layers are forming clusters as soon

as the incompatibility with the solvent exceeds a certain threshold (Figure 4). Their shapes, forming either droplike "dimples" or rather extended, stripelike "ripples", are functions of the solvent selectivity, grafting density, and chain length. The lateral structure factor delivers evidence about how the size of these clusters depends on the chain length (Figure 3). This, in turn, explains why the height of the lower layer does not, as expected, scale linearly with the chain length N: The size distribution of the corresponding domains, i.e., the roughness of the layer, is itself a function of the chain length. Figure 2 suggests an empirical $\sim N^{2/3}$ scaling of the layer thickness at high solvent selectivity. But this is limited to a regime in which the poor solvent phase does not form a closed film on top of the substrate, and this regime has to move into the usual $\sim N$ regime at sufficiently high grafting densities or beyond a certain chain length.

The switching time is scaling as $\sim N^2$ with the chain length, just like the Rouse relaxation time of the end-to-end vector of isolated chains (Figure 7) and unlike the $\sim N^3$ scaling of vertical chain relaxation in equilibrium. The relaxation of both layers is partially decoupled, and both display different relaxation times, since the driving forces are either enthalpic (shrinking of the formerly swollen layer inside the poor solvent) or entropic (swelling of the formerly collapsed poor solvent layer) and hence of entirely different nature. The actual switching times should not be regarded as realistic, however, because in a true experimental situation the solvent cannot be exchanged instantaneously as it was done in the present simulation. Instead, the new solvent has to replace the old solvent while penetrating the brush layer in a diffusive process, which itself would take a significant time.

We have compared the switching times for the case of $N = 64$ and $\epsilon = 1$ with different grafting patterns, including a checkerboard, alternating rows of **A** and **B** species, and also a random occupation of both species on a Cartesian pattern. The observed switching times did coincide within a 10% error margin, too insignificant to be regarded as a clear signature for a dependence on the grafting pattern, when considering the accuracy achievable with this method. It can therefore be concluded that no significant variation of the switching dynamics with the grafting pattern was observed.

Finally, hydrodynamic correlation effects were entirely neglected in the present simulations. Being a semidilute polymeric system, these are generally expected to be screened on the length scale of correlation blobs. The latter blobs would therefore exhibit Rouse dynamics, although diffusion on short length scales would display hydrodynamic screening. The Rouse scaling would then remain unaffected; only an additional prefactor would arise due to hydrodynamics, which is tolerable for a coarse-grained model as used in the simulation. It should be noted, however, that the collective vertical motion of microdomains during the switching could in fact qualitatively differ from the diffusion of correlation blobs, and hence the possibility of certain hydrodynamic correlations over length scales exceeding the blob size cannot be entirely excluded. However, when considering the size of the system, an explicit simulation of hydrodynamic correlations would be beyond the scope of the current investigation and has to be postponed to future projects.

Acknowledgment. This work was partly supported by the National Science Foundation of China under Grant No. 10225420. G.-L. He thanks J.-U. Sommer for the hospitality during a research stay at the IPF Dresden.

References and Notes

(1) Creton, C. *MRS Bull.* **2003**, *28*, 434.
(2) Liu, Y.; Chen, X.; Xin, J. *Nanotechnology* **2006**, *17*, 3259.
(3) Li, N.; Veldhuis, S. C.; Yamamoto, K. *Mach. Sci. Technol.* **2007**, *11*, 45.
(4) Marko, J.; Witten, T. *Phys. Rev. Lett.* **1991**, *66*, 1541.
(5) Marko, J.; Witten, T. *Macromolecules* **1992**, *25*, 296.
(6) Mueller, M. *Phys. Rev. E* **2002**, *65*, 030802.
(7) Minko, S.; Mueller, M.; Usov, D.; Scholl, A.; Froeck, C.; Stamm, M. *Phys. Rev. Lett.* **2002**, *88*, 035502.
(8) Sidorenko, A.; Minko, S.; Schenk-Meuser, K.; Duschner, H.; Stamm, M. *Langmuir* **1999**, *15*, 8349.
(9) Minko, S.; Usov, D.; Goreshnik, E.; Stamm, M. *Macromol. Rapid Commun.* **2001**, *22*, 206.
(10) Lemieux, M.; Usov, D.; Minko, S.; Stamm, M.; Shulha, H.; Tsukruk, V. *Macromolecules* **2003**, *36*, 7244.
(11) Motornov, M.; Sheparovych, R.; Lupitskyy, R.; MacWilliams, E.; Hoy, O.; Luzinov, I.; Minko, S. *Adv. Funct. Mater.* **2007**, *17*, 2307.
(12) Chervanyov, A.; Heinrich, G. *Mater. Res. Soc. Symp. Proc.*, **2007**, 947 (0947-A10–02).
(13) Soga, K. G.; Zuckermann, M. J.; Guo, H. *Macromolecules* **1996**, *29*, 1998.
(14) Wenning, L.; Mueller, M.; Binder, K. *Europhys. Lett.* **2005**, *71*, 639.
(15) Santer, S.; Kopyshev, A.; Donges, J.; Ruehe, J.; Jiang, X.; Zhao, B.; Mueller, M. *Langmuir* **2007**, *23*, 279.
(16) Yin, Y.; Jiang, R.; Li, B.; Jin, Q.; Ding, D.; Shi, A.-C. *J. Chem. Phys.* **2008**, *129*, 154903.
(17) Mao, Y.; Liu, D.; Wang, S.; Wang, S. L. W.; Yang, Y.; Ouyang, Q.; Jiang, L. *Nucleic Acids Res.* **2007**, *35*, e33.
(18) Kremer, K.; Grest, G. *J. Chem. Phys.* **1990**, *92*, 5057.
(19) Plimpton, S. *J. Comput. Phys.* **1995**, *117*, 1 (http://lammps.sandia.gov/).
(20) He, G.; Merlitz, H.; Sommer, J.; Wu, C. *Eur. Phys. J. E* **2007**, *24*, 325.
(21) Halperin, A. In Bruinsma, R., Rabin, Y., Eds.; *Soft Order in Physical Systems*; NATO ASI Series; Plenum Press: New York, 1994; p 33.
(22) Baulin, V. A.; Halperin, A. *Macromol. Theory Simul.* **2003**, *12*, 549.
(23) Hoffmann, A.; Sommer, J.-U.; Blumen, A. *J. Chem. Phys.* **1997**, *106*, 6709.
(24) He, G.; Merlitz, H.; Sommer, J.; Wu, C. *Macromolecules* **2007**, *40*, 6721.
(25) deGennes, P. *Adv. Colloid Interface Sci.* **1987**, *27*, 189.
(26) Alexander, S. *J. Phys. (Paris)* **1977**, *38*, 977.
(27) Rouse, P. *J. Chem. Phys.* **1953**, *21*, 1272.
(28) Johner, A.; Joanny, J. F. *J. Chem. Phys.* **1993**, *98*, 1647.
(29) Lai, P.-Y.; Binder, K. *J. Chem. Phys.* **1992**, *97*, 586.

MA8019877